Journal of Southeast University (English Edition) Vol. 39, No. 1, pp. 89 - 97 Mar. 2023 ISSN 1003—7985

Ameliorating the vibratory roller's ride quality based on QZSS and the seat's semi-active suspension

Nguyen Van Liem[1,2] Zhang Jianrun[3] Zhou Huaxiang[1,2]

([1]School of Mechanical and Electrical Engineering, Hubei Polytechnic University, Huangshi 435003, China)
([2]Hubei Key Laboratory of Intelligent Conveying Technology and Device, Hubei Polytechnic University, Huangshi 435003, China)
([3]School of Mechanical Engineering, Southeast University, Nanjing 211189, China)

Abstract: A combination of the semi-active suspension (SAS) and quasi-zero stiffness structure (QZSS) is proposed for a seat suspension to improve the ride comfort of a vibratory roller. A 3D vehicle dynamic model is built to assess the isolation performance of the seat's SAS combined with the QZSS under a vehicle's different working conditions on elastoplastic soil. An experimental investigation is also used to verify the accuracy of the model. The weighted root mean square (a_{ws}) and power-spectral-density (PSD) accelerations of the driver's seat are selected as the evaluation indexes. The research results show that the seat's SAS significantly improves the vibratory roller's ride comfort compared to the seat's passive suspension (PS), whereas the QZSS added into the seat's PS improves the ride comfort better than the seat's SAS. In particular, with the QZSS embedded in the seat's SAS, the values of a_{ws} and the maximum PSD of the driver's seat are strongly reduced by 75.7% and 74.3% compared to the seat's PS, respectively. Therefore, the QZSS embedded in the seat's SAS should be used to further enhance the ride comfort of the vibratory roller.

Key words: vibratory roller; quasi-zero stiffness structure; semi-active suspension; ride comfort

DOI: 10.3969/j.issn.1003 - 7985.2023.01.011

With vibratory rollers working on the elastoplastic soil ground, the vibration responses of the driver's seat in the vertical direction and cab shaking are great. These values strongly influence the ride quality and working performance of drivers[1-2]. Thus, to ameliorate the ride quality of vibratory rollers, a cab's isolation systems of vibratory rollers were examined by applying hydraulic mounts (HMs)[3]. Moreover, based on optimal control methods, the semi-active isolation systems of a vibratory roller cab were studied and controlled[3-4]. As a result, the ride quality of the driver was remarkably ameliorated compared to the cab's passive isolation systems. However, according to the standard of ISO 2631-1[5], the vibration of the driver's seat in the vertical direction was still high, especially under the condition of the vehicle compacting on elastoplastic grounds. To solve this problem, the seat's passive suspensions (PS) of vibratory rollers need to be improved.

The existing studies of the driver's seat suspension showed that the semi-active suspension (SAS) of the driver's seat optimized or controlled could improve the ride comfort better than that of the seat's PS[6-7], especially with the fuzzy control. Moreover, the driver's seat suspension embedded by the quasi-zero stiffness structure (QZSS) was studied to improve the vehicle's ride comfort[8-9]. The QZSS was also tested to validate its actual performance[10]. Moreover, the dynamic parameters of the QZSS were optimized to enhance ride comfort[11]. The study results show that the seat's ride comfort was greatly improved by the seat's PS added by the QZSS. However, the 1D vehicle dynamic model was only used to evaluate the performance of the seat's SAS and QZSS[6-11], whereas the actual structure of the vehicle is 3D. Therefore, the performance of the SAS and QZSS has not been fully reflected yet. Furthermore, based on the isolation performance of the SAS and QZSS, a combination of the SAS and QZSS can further improve the ride comfort of the driver's seat. However, this issue has not been considered yet. In addition, in the models of the SAS and QZSS, the vibration excitation of the rigid road surface was only used to assess the performance of the SAS and QZSS. However, with off-road vibratory rollers, off-road vehicles mainly travel on deformable terrain and compress elastoplastic soils. Thus, the stability and isolation performance of the SAS and QZSS could be affected by the excitation of deformable soil grounds. However, this issue has not been studied and evaluated yet.

To solve the above existing problems and enhance the ride comfort of vibratory rollers, a QZSS embedded in a seat's SAS is proposed and researched. A 3D dynamic model of a vibratory roller was built to evaluate the isolation performance of the seat's SAS added by the QZSS

Received 2022-06-20, **Revised** 2022-12-18.

Biographies: Nguyen Van Liem (1986—), male, doctor; Zhang Jianrun (corresponding author), male, doctor, professor, zhangjr@seu.edu.cn.

Foundation items: The National Key Research and Development Plan (No. 2019YFB2006402), Key Scientific Research Project of Hubei Polytechnic University (No. 22xjz02A).

Citation: Nguyen Van Liem, Zhang Jianrun, Zhou Huaxiang. Ameliorating the vibratory roller's ride quality based on QZSS and the seat's semi-active suspension[J]. Journal of Southeast University (English Edition), 2023, 39(1): 89 - 97. DOI: 10.3969/j.issn.1003 - 7985.2023.01.011.

under various conditions of the vibratory roller. In addition, an experimental study of the vibratory roller was performed to enhance the reliability of the mathematical model and calculation result. The decrease in the weighted root mean square and power-spectral-density (PSD) accelerations of the driver's seat to enhance the ride comfort of the vibratory roller was selected as the evaluation index.

1 Mathematical Model

A 3D nonlinear dynamic model of a vibratory roller with 9 degrees of freedom considering the interaction between wheels and elastoplastic soil ground was built to evaluate the vehicle's ride comfort (see Fig. 1).

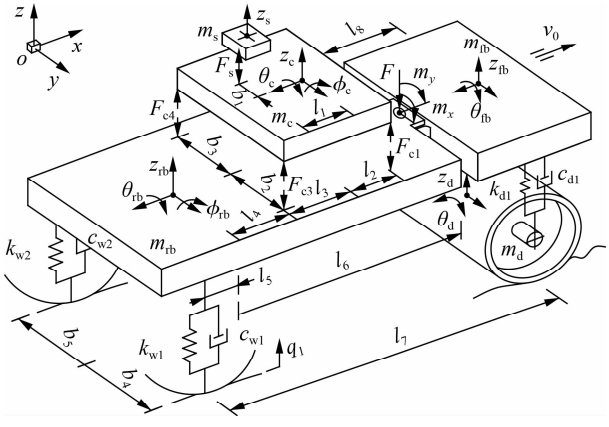

Fig. 1 Vibratory roller's dynamic model

In Fig. 1, m_ϑ and z_ϑ are the mass and displacement of the driver's seat, cab, front/rear vehicle floor, and drum; ϕ_c and ϕ_{rb} are the pitching angles of the cab and rear vehicle floor, respectively; θ_δ is the rolling angles of the cab, front/rear vehicle floor, and drum; k_{dj}, k_{wj} and c_{dj}, c_{wj} are the stiffness and damping coefficients of the drum's isolations and wheels, respectively; F_s is the seat's force response; F_{ci} are the force responses of the cab's HM; l_1 to l_8 and b_1 to b_5 are the distances of the vehicle in the x- and y-directions; and v_0 and q_w are the moving speed and vibration excitation of the vehicle, respectively ($i = 1, 2, 3, 4$; $j = 1, 2$; ϑ = s, c, fb, rb, and d; δ = c, fb, rb, and d).

To simplify the calculation process of the motion equations of the vehicle, the following assumptions are given: 1) Due to the vehicle's vibration being generated by the drum/wheel and deformable terrain interaction in the vertical direction, it is assumed that the longitudinal and horizontal impacts are very small and ignored. 2) At the swivel joint between the front and rear vehicle floor, there are two yawing and rolling motions. Other motions are constrained. 3) The deformation of the cab floor and rear vehicle floor is very small. Moreover, the displacements of the driver's seat, cab floor, and front/rear vehicle floor around their equilibrium position are very small.

Based on the vehicle dynamic models in Fig. 1 and by applying Newton's second law of motion, the vibratory roller's motion equations can be represented in the matrix form as

$$\boldsymbol{M}\ddot{\boldsymbol{Z}} + \boldsymbol{C}\dot{\boldsymbol{Z}} + \boldsymbol{K}\boldsymbol{Z} = \boldsymbol{F}(t) \tag{1}$$

where $\boldsymbol{M}$, $\boldsymbol{C}$, and $\boldsymbol{K}$ are the mass, damping, and stiffness matrices, respectively; $\boldsymbol{Z}$ is the displacement vector; and $\boldsymbol{F}(t)$ is the exciting force vector.

The excitation forces of F_s, F_{ci}, F_{dj}, and F_{wj} in $\boldsymbol{F}(t)$ are determined as follows.

1) F_s of the seat's suspension is determined by the process presented in Section 2.

2) F_{ci} of the cab's isolation: The cab's isolation was equipped with four rubber mounts to reduce its vibration. Existing research shows that a cab's HM improved the vibratory roller's ride comfort better than rubber and pneumatic mounts[1-2]. Thus, the cab's isolation was used by the HM to improve the vehicle's ride comfort. The lumped parameter model is plotted in Fig. 2, where k_r and c_r are the stiffness and damping coefficients of the rubber mount, respectively, and c_h is the damping coefficient of the fluid of the HM.

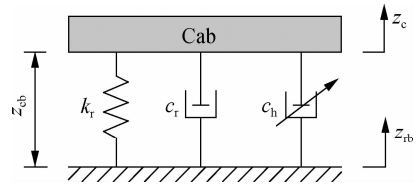

Fig. 2 The model of a cab's HM

3) F_{ci} of the cab's HM is expressed by[3-4]

$$\left.\begin{aligned} F_{ci} &= k_{ci} z_{cbi} + c_{ci}\dot{z}_{cbi} + c_{hi}\dot{z}_{cbi} \mid \dot{z}_{cbi} \mid \\ z_{cbi} &= [\, z_c - z_{rb} + (-1)^{u+1} l_{u+1}\phi_c - \ldots - \\ &\quad l\phi_{rb} + (-1)^{i+1} b_v(\theta_c - \theta_{rb}) \,] \end{aligned}\right\} \tag{2}$$

where if $i = 1, 2$, then $u = 1$, $l = l_2 + l_3 + l_4$, and $v = i + 1$; and if $i = 3, 4$, then $u = 2$, $l = l_4$, and $v = i - 1$.

4) F_d of the drum's isolation: The vibratory roller uses most of its time to work on elastoplastic soil. Thus, according to Ref. [1], an interaction model of the drum and elastoplastic soil was established, as shown in Fig. 3, where k_{se}, k_{ps}, and c_{se} are the elastic stiffness, compression stiffness, and compression damper, respectively.

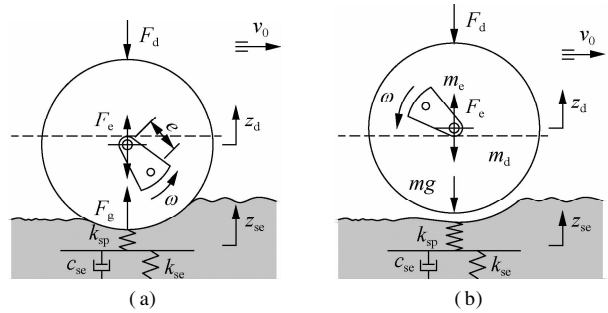

Fig. 3 The interaction model of the drum and elastoplastic soil. (a) Loading phase; (b) Drum-hop phase

Based on the research results of Ref. [1], the calculation method for the relative stiffness and damper to describe the elastoplastic property of the soil ground was given based on two indexes, i. e., plasticity factor ε and damping ratio γ:

$$\varepsilon = \frac{k_{ps}}{k_{ps} + k_{se}}, \quad \gamma = \frac{c_{se}}{k_{ps}} \tag{3}$$

The mutation parameter of ε is from 0 to 1. The value $\varepsilon = 0$ achieved as $k_{ps} = 0$ refers to the purely plastic soil property, which degrades the loss of the drum-soil contact. The value $\varepsilon = 1$ refers to an ideal elastic soil property achieved as $k_{ps} \to \infty$.

Under the interaction between the rigid drum and elastoplastic soil ground, the drum's vibration equation is expressed by[1-2]

$$\left.\begin{aligned} F_d &= k_{dj}(z_{fbj} - z_{dj}) + c_{dj}(\dot{z}_{fbj} - \dot{z}_{dj}) \\ F_g &= k_{ps}[z_d - (q - z_{es})] = c_{es}\dot{z}_{es} + k_{es}z_{es} \\ m_d\ddot{z}_d &= F_d - F_g + F_e \end{aligned}\right\} \tag{4}$$

where $z_{fbj} - z_{dj} = z_{fb} - z_d + (-1)^j b_{3+j}(\theta_{fb} - \theta_d)$; $j = 1, 2$.

In a vibration cycle of the drum and elastoplastic soil interaction, two or three distinct phases (i. e., loading, unloading, and drum-hop phases) occur in the motion of the drum, which is described as follows:

Loading phase: The soil ground is compressed by the drum. Thus, its density is increased, and it becomes elastic. The stiffness of k_{se} and k_{sp} is increased, whereas the compression damper c_{se} is reduced. To describe the relationship of ε, γ, and z_d, the drum's motion equation is given by[1]

$$\left.\begin{aligned} &\varepsilon\gamma m_d \dddot{z}_d + m_d\ddot{z}_d = \varepsilon\gamma\dot{F}_d + F_d - \varepsilon c_{es}\dot{z}_d + \cdots \\ &\qquad + (\varepsilon - 1)k_{ps}z_d + \varepsilon\gamma\dot{F}_e + F_e \\ &F_e = m_e e\omega^2 \sin\omega t \end{aligned}\right\} \tag{5}$$

Unloading phase: The drum moves upward, and the soil ground is restored. The drum's equation is written as

$$m_d\ddot{z}_d = F_d - c_{es}\dot{z}_d + F_e \tag{6}$$

Drum-hope phase: The soil ground has become elastic, and the drum easily separates from the soil ground surface. The drum's equation is written as

$$m_d\ddot{z}_d = F_d + mg + F_e \tag{7}$$

From Eqs. (4) to (7), F_d is then determined.

5) F_w of the wheel-deformable terrain contact: In the condition of a vehicle traveling on a deformable terrain, under the effect of the static load and dynamic load of the wheels, the contact region of the wheel and terrain could have two deformations: 1) only deformation of the terrain (region of ba) and 2) deformation of the wheel and terrain (region of $b'ob$), as illustrated in Fig. 4. m_w and r_w are the wheels' mass and radius, respectively; p and τ are the press and stress of the deformable soil ground at point x; z_w, z_{w0}, and z_x are the wheels' displacement, wheel's static deformation, and terrain's sinkage, respectively; and q is the excitation of the terrain surface.

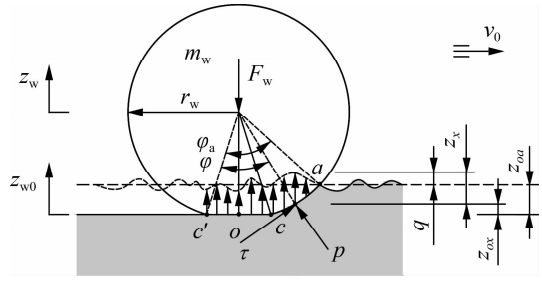

Fig. 4 Model of the wheel and soil ground contact

Based on the study results in Refs. [12 − 13], the generated force of p and τ in the deformable regions of ba and $b'ob$ is expressed as follows:

$$\left.\begin{aligned} F_{gw} &= \int_0^{\varphi_a} B_w r_w (p\cos\varphi + \tau\sin\varphi)\,\mathrm{d}\varphi \\ p &= \left(\frac{k}{B_w} + k_\theta\right) z_x^n \\ \tau &= (C + p\tan\theta)(1 - \mathrm{e}^{-j/K}) \end{aligned}\right\} \tag{8}$$

where $z_x = z_{oa} + q - z_{ox} = q + z_w - z_{w0} - z_{ox}$; n is the sinkage exponent; k is the terrain's sinkage stiffness; k_φ is the terrain's internal friction stiffness; B_w is the wheel's width; and C is the soil cohesion coefficient.

Thus, the force responses of the wheels are calculated by

$$\left.\begin{aligned} F_{wj} + F_{gwj} - m_{wj}g = 0 \\ F_{wj} = k_{wj}Z_j + c_{wj}\dot{Z}_j \end{aligned}\right\} \tag{9}$$

where $Z_j = z_{rb} - l_5\varphi_{rb} - z_{wj} + (-1)^j b_{j+3}\theta_{rb}$, $j = 1 - 2$.

To determine F_{wj}, the vibration excitation of q of the deformable terrain needs to be computed. Based on the standard of ISO/TC108/SC2/WG4[14], the PSD of the terrain surface roughness $S(n)$ is written as[14-15]

$$S(n) = S(n_0)\left(\frac{n}{n_0}\right)^{-\delta_0}, \quad \delta_0 = \begin{cases} 2.25 & n > n_0 \\ 3 & n \leqslant n_0 \end{cases} \tag{10}$$

where $S(n_0)$ is the reference density of the terrain surface roughness, and n_0 is the reference spatial frequency.

Based on the white noise signal of the random function (w) and $S(n)$ of the terrain surface roughness at a moving speed of the vibratory roller (v_0), the vibration excitation of q is calculated as follows[7]:

$$\dot{q} + 2\pi n_0 v_0^2 q = 2\pi n_0 \sqrt{S(n_0)v_0}\, w \tag{11}$$

Four different levels of the terrain surface roughness established via their PSD value, i. e., good surface, medium surface, poor surface, and very poor surface, were proposed by Mitschke[16] to calculate q. Therefore, q can be determined by selecting one of four different levels of the terrain surface roughness.

2 SAS of the Driver's Seat

2.1 Seat's SAS added by the QZSS

QZSS's term is as follows: With a structure designed by the elastic spring, if the compressive force F increases, the deformation z also increases and vice versa. The relationship between F and z is determined by $F = kz$. Thus, k is defined as the elastic spring's "positive stiffness," as plotted in Fig. 5(a). Conversely, with a structure designed by two symmetrical springs or elastic bars, if the compressive force F increases, the deformation z reduces and vice versa. Thus, k is defined as the elastic spring's "negative stiffness," as plotted in Fig. 5(b). With a structure designed by the combination of "positive stiffness" and "negative stiffness," if the deformation z increases or reduces, the force F is always a constant. Thus, k is defined as "quasi-zero stiffness," as plotted in Fig. 5(c). This QZSS is then studied and applied to the seat suspension of the vibratory roller.

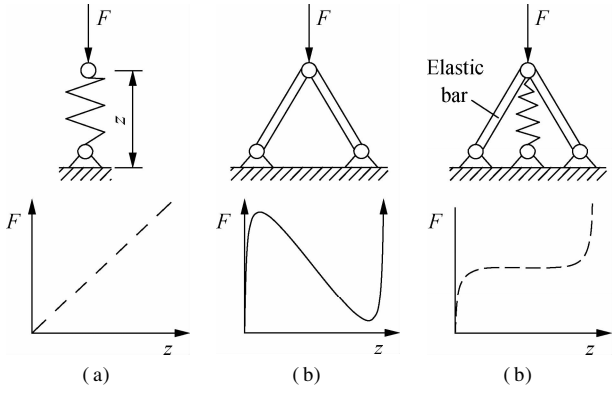

Fig. 5 The model and characteristics of the QZSS. (a) QZSS's model; (b) Characteristic of the restoring force-deformation force

Model of the seat's SAS added by the QZSS: The PS of the vibratory roller seat was designed using a passive steel spring and damper[2-3], as modeled in Fig. 6(a). c_s and k_s are the passive damping and stiffness parameters of the seat's PS, respectively.

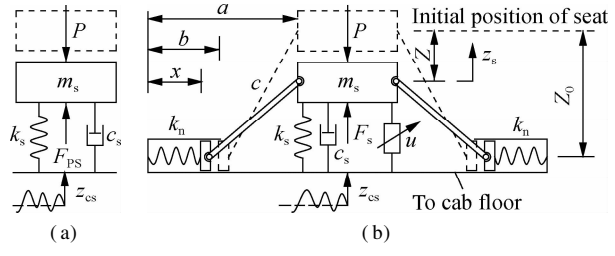

Fig. 6 Driver's seat suspension model. (a) Seat's PS; (b) seat's SAS added by the QZSS

Based on the dynamic models of the vehicle in Fig. 1 and the PS of the driver's seat in Fig. 6(a), F_s of the PS is expressed by

$$\left.\begin{aligned} F_s &= F_{PS} = k_s(z_s - z_{cs}) + c_s(\dot{z}_s - \dot{z}_{cs}) \\ z_{cs} &= z_c - l_1\varphi_c - b_1\theta_c \end{aligned}\right\} \quad (12)$$

The vibratory roller's ride comfort was mainly improved based on the optimization and control of the cab isolations, whereas the seat's suspension was always used by the PS[3-4]. With this model, the ride comfort of the driver's seat is difficult to be ensured based on ISO 2631-1[5]. To improve the vehicle's ride comfort, the seat's PS was added by a semi-active damping parameter (C_{semi}) and the QZSS, as modeled in Fig. 6(b).

In Fig. 6(b), a, b, and c are the distance between the wall and seat, the initial length of the horizontal spring, and the length of the hard guide bar used to link between the horizontal spring and seat, respectively; Z_0 and x are the distance between the cab's floor and initial position of the seat and the length after deformation of the horizontal spring; and k_n is the stiffness parameter of the horizontal springs. Under the impact of the static load $P = m_s g$ on the driver's seat, the suspension deformation of the seat is generated by Z. Thus, F_s is determined by

$$\left.\begin{aligned} F_s &= F_{semi} + F_r \\ F_{semi} &= (C_{semi} + c_s)\dot{Z} \\ F_r &= k_s Z + \frac{2k_n(b-x)(Z_0 - Z)}{a-x} \end{aligned}\right\} \quad (13)$$

where F_{semi} is the semi-active damping force, and F_r is the restoring forces of the springs k_s and k_n.

Based on theinitial and equilibrium positions of the driver's seat in Fig. 6(b), x and Z_0 are calculated as

$$\left.\begin{aligned} x &= a - \sqrt{c^2 - (Z_0 - Z)^2} \\ Z_0 &= \sqrt{c^2 - (a-b)^2} \end{aligned}\right\} \quad (14)$$

By substituting Eq. (14) into Eq. (13), F_s is rewritten by

$$F_s = F_{semi} + k_s Z + \alpha k_s \left[\frac{1-\beta_2}{\sqrt{\beta_1^2 - (_0 - Z)^2/b^2}} + 1\right](Z_0 - Z) \quad (15)$$

where $\alpha = 2k_n/k_s$, $\beta_1 = c/b$, and $\beta_2 = a/b$ are the stiffness ratios and geometrical dimension ratios of the QZSS.

Under the excitation of z_{cs} on the seat's suspension, the seat's vibration was then generated by z_s (see Fig. 6(b)). Thus, the seat's vibration equation is written as

$$m_s\ddot{z}_s = -\left[(C_{semi} + c_s)(\dot{z}_s - \dot{z}_{cs}) + \ldots + k_s(z_s - z_{cs}) + \alpha k_s(\Lambda + 1)(Z_0 - Z)\right] \quad (16)$$

where $\Lambda = (1 - \beta_2)/\sqrt{\beta_1^2 - (Z_0 - Z)^2/b^2}$; $Z_0 - Z = z_s - z_{cs}$; and z_{cs} is given in Eq. (12).

Eq. (16) is used to evaluate the performance of the seat's SASS added by the QZSS.

2.2 Control of the seat's SAS using fuzzy control

The fuzzy controller can control suspension systems under various operating conditions, and its control performance is good and stable. However, its performance is

strongly dependent on control rules[3,7]. To enhance the performance of the fuzzy controller, its control rules optimized by the genetic algorithm were used to control C_{semi} of the seat's SAS. The fuzzy control was designed by two input variables of the vertical displacement "$e = z_s - z_{es}$" and velocity "ec = $\dot{e}$" of the driver seat's suspension and one output variable of C_{semi}. The model of the fuzzy control for the vibratory roller is plotted in Fig. 7.

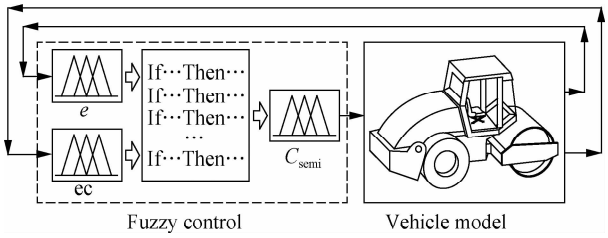

Fig. 7 Control model of the seat's SAS using the fuzzy control

The structure of the fuzzy control includes the fuzzification interface, fuzzy inference system, and defuzzification interface. First, crisp values in the fuzzification interface are transformed into linguistic variables (LVs). The fuzzy inference system is then used in accordance with inference rules. Finally, LVs are transformed back to crisp values via defuzzification for use by a physical plant[17]. The fuzzy control is designed as follows:

1) Define and set the LVs of the input/output values. The LVs of e and ec are classified as negative-big (NB), negative-small (NS), zero (Z), positive-small (PS), and positive-big (PB). Moreover, the LVs of C_{semi} are classified as small (S), medium-small (MS), medium (M), medium-big (MB), and big (B). The numerical values of the LVs are defined in Tab. 1. **Tab. 1** Language variables and thetheir numerical values

Inputvalue			Output value	
LV	e	ec	LV	$C_{semi}/10^3$
NB	−0.02	−0.30	S	0.1
NS	−0.01	−0.15	MS	0.4
Z	0	0	M	0.8
PS	0.01	0.15	MB	1.2
PB	0.02	0.30	B	1.5

2) Set the membership function. The membership function of the input/output values is used by the triangular function (see Fig. 7).

3) Set the control rule of the fuzzy control. Based on the optimal control rules of the fuzzy control[18], as listed in Tab. 2, the control rules are applied to control C_{semi}. The control rule of e, ec, and C_{semi} is then established by the following:

1) If e is NB and ec is NB, then C_{semi} is B.

2) If e is NB and ec is NS, then C_{semi} is MB.

⋮

25) If e is PB and ec is PB, then C_{semi} is B.

The centroid method and minimum function established in the fuzzy control tool were then chosen to calculate C_{semi} based on the control rule and parameter values of e and ec.

Tab. 2 The optimal control rule of the fuzzy control

ec	e				
	NB	NS	Z	PS	PB
NB	B	B	MB	S	S
NS	MB	M	MS	S	MS
Z	MB	MS	S	MS	M
PS	MS	S	MS	M	B
PB	S	MS	MS	M	B

3 Results and Discussions

3.1 Evaluation index

The isolation performance of the suspension systems was mainly evaluated using three indexes, namely, ride quality, suspension deformation, and road friendliness[3-4,7]. The driver's seat ride quality was evaluated via the weighted root-mean-square seat acceleration (a_{ws}) in the time region[4-5,9]. In addition, based on ISO 2631-1[5], the PSD acceleration was applied to evaluate the effect of the vibration on the human body's endurance limit in the low-frequency region, especially at a low-frequency region from 0.5 to 4 Hz. a_{ws} of the driver's seat is written as[5,7]

$$a_{ws} = \left(T^{-1} \int_0^T \ddot{z}_s^2 \mathrm{d}t \right)^{0.5} \tag{17}$$

where $\ddot{z}_s$ is the acceleration of the driver's seat, and T is the simulation time.

Thus, to evaluate the vehicle's ride quality and the performance of the seat's SAS added by the QZSS, the seat's a_{ws} and maximum PSD value were selected as the evaluation indexes.

3.2 Performance of the seat's SASS added by the QZSS

The vibratory roller mainly works on elastoplastic soil. Thus, to evaluate the performance of the seat's SAS added by the QZSS on improving the vehicle's ride comfort, the optimal parameters of the QZSS in Tab. 3[9], the lumped parameters of the vibratory roller in Tab. 4[4], the parameters of the elastoplastic soil ground at the rigid drum and wheel in Tab. 5[1-3], and the parameters of a poor level of the soil ground surface in Tab. 6[16] were chosen to simulate at the vibratory roller's low velocity $v_0 = 1.67$ m/s under excitation of the drum $f = 28$ Hz. The simulation result of the seat's acceleration under four different cases of the seat's suspension, namely, 1) seat's PS, 2) seat's SAS, 3) seat's PS added by the QZSS (PS + QZSS), and 4) seat's SAS added by the QZSS (SAS + QZSS), is plotted in Fig. 8.

Tab. 3 QZSS's optimal parameters

Parameter	a/m	k_s/(kN · m^{-1})	c_s/(kN · s · m^{-1})	α	β_1	β_2
Value	0.286	5.8	120	0.63	0.73	1.17

Tab. 4 The dynamic parameters of the vibratory roller

Parameter	Value	Parameter	Value
m_s/kg	85	$c_{w1,2}$/(kN · s · m^{-1})	4.0
m_c/kg	891	l_1/m	0.383
m_{fb}/kg	2 822	l_2/m	0.1
m_{rb}/kg	4 464	l_3/m	0.524
m_d/kg	4 378	l_4/m	0.136
$k_{c1,2}$/(MN · m^{-1})	0.91	l_5/m	0.6
$k_{c3,4}$/(MN · m^{-1})	0.12	l_6/m	0.76
$k_{d1,2}$/(MN · m^{-1})	3.9	l_7/m	0.9
$k_{w1,2}$/(MN · m^{-1})	0.5	l_8/m	1.5
$c_{c1,2}$/(N · s · m^{-1})	218	b_1/m	0.55
$c_{c3,4}$/(N · s · m^{-1})	29	b_2/m	0.7
$c_{h1,2}$/(kN · s^2 · m^{-2})	20	b_3/m	0.68
$c_{h3,4}$/(kN · s^2 · m^{-2})	4.5	b_4/m	0.945
$c_{d1,2}$/(kN · s · m^{-1})	2.9	b_5/m	0.945

Tab. 5 The parameters of the elastoplastic soil ground

Off-road surfaces	Parameter	Value
Elastoplastic soil ground under the rigid drum	ε	0.87
	k_{ps}/(MN · m^{-1})	283
	k_{es}/(MN · m^{-1})	42.3
	c_{es}/(kNs · m^{-1})	37.1
Deformable soil ground under the wheels	θ/(°)	29.8
	k/(N · m^{-n-1})	6
	k_θ/(MN · m^{-n-2})	5.88
	C/Pa	310

Tab. 6 The parameters of a poor surface of the soil ground

Parameter	Value
$S(n_0)$/(cm^3 · cycle^{-1})	3 782.5
δ_0	2.14

Fig. 8(a) reveals that the driver's seat acceleration with the seat's SASS is lower than that of the seat's PS. This result is attributed to the active damping parameter C_{semi} in Eq. (13) controlled via the fuzzy control to decrease the driver's seat acceleration. With the PS + QZSS, the driver's seat acceleration is remarkably decreased in comparison with the seat's SAS and PS. This result is attributed to the effect of the restoring force F_r of the springs described in Eq. (13). The existing studies demonstrate that the performance of the seat's PS added by the QZSS in improving the seat's ride comfort is better than the seat's PS without the QZSS[8–11]. Moreover, this research indicates that the driver's seat acceleration with the PS + QZSS is reduced in comparison with the seat's SAS. Hence, the QZSS improves the ride comfort better than the SAS. With the SAS + QZSS, the driver's seat acceleration is decreased as compared to the PS + QZSS. This result is because of the impact of C_{semi} and F_r in Eq. (13).

In addition, the calculation results in Fig. 8(b) indicate that a_{ws} with the seat's SAS, PS + QZSS, and SAS + QZSS

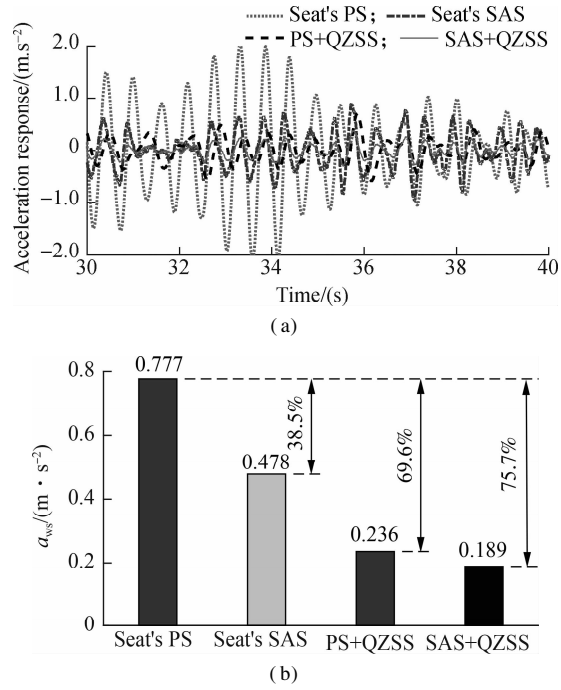

Fig. 8 The driver's seat's vibration response. (a) Acceleration response; (b) Weighted root-mean-square acceleration

has been strongly reduced by 38.5%, 69.6%, and 75.7% compared to the seat's PS, respectively, especially with the SAS + QZSS. Thus, the ride comfort of the vehicle with the SAS + QZSS is better improved in comparison with the seat's SAS and PS + QZSS.

The driver's seat vibration response in the low-frequency range is also presented to compare the performance between the seat's SAS, PS + QZSS, and SAS + QZSS, as shown in Fig. 9. The result shows that the PSD acceleration of the driver's seat with the seat's SAS, PS + QZSS, and SAS + QZSS is also obviously decreased compared to the seat's PS, particularly with the SAS + QZSS. This result is also attributed to the impact of C_{semi} and F_r in Eq. (13). In particular, at a low-frequency range of 0.5 to 4.0 Hz, which strongly influences the safety and health of the driver[7], the results in Tab. 7 indicate that the maximum value of the PSD seat acceleration with the seat's SAS, PS + QZSS, and SAS + QZSS is markedly

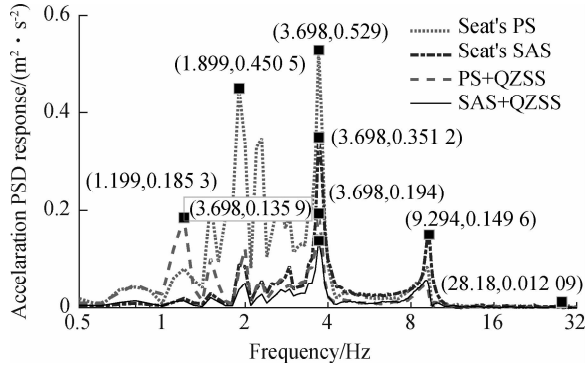

Fig. 9 PSD acceleration response of the driver's seat

Tab. 7 The maximum PSD acceleration of the driver's seat

Isolations	Frequency/Hz	Maximum PSD/($m^2 \cdot s^{-3}$)
Seat's PS	3.698	0.529
Seat'sSAS	3.698	0.351
PS + QZSS	3.698	0.194
SAS + QZSS	3.698	0.136

decreased by 33.6%, 63.3%, and 74.3% in comparison with the seat's PS, respectively, especially with the SAS + QZSS. Thus, the QZSS embedded in the seat's SAS greatly ameliorates the driver's ride comfort in terms of frequency and time ranges. However, the performance of the SAS + QZSS only evaluates under one operating condition of the off-road vibratory roller. To fully assess the stability and performance of the SAS + QZSS, the various values of the vehicle's velocity and driver's mass should also be simulated and evaluated.

3.3 Performance under various conditions

Under the same simulation conditions of the vibratory roller in Section 3.2, the change in the vehicle's speed and driver's mass was used to assess the stability and performance of the SAS + QZSS. With the change in the driver's mass $m_s = [60, 65, \ldots, 100]$ (kg), the calculation results are depicted in Fig. 10(a). The results show that a_{ws} with the seat's PS, PS + QZSS, and SAS + QZSS has been decreased when the value of m_s is increased and vice versa. Therefore, the ride comfort of the driver is significantly influenced by the change in m_s. However, using the SAS + QZSS, a_{ws} was not only reduced compared to the seat's SAS and PS + QZSS but also became stable under the change in the driver's mass.

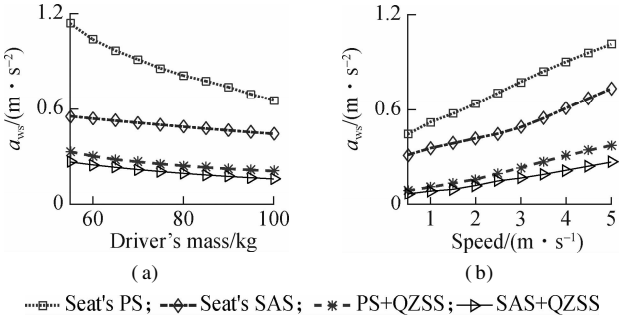

Fig. 10 Seat's vibration response under different conditions. (a) Change in the driver's mass; (b) Change in the vehicle's moving speed

Similarly, the calculation results with the change in the vehicle's speed $v_0 = [1.0, 1.5, \ldots, 5.0]$ (m/s) are depicted in Fig. 10(b). The results show that when the vehicle's speed is increased, a_{ws} with the seat's PS, PS + QZSS, and SAS + QZSS is also increased and vice versa. Thus, the ride comfort of the driver is remarkably decreased when the moving speed of the vibratory roller is increased. Using the SAS + QZSS, the result of a_{ws} is smaller than that of the seat's SAS and PS + QZSS under all the different moving speeds of the vehicle. Thus, the QZSS embedded in the seat's SAS can markedly enhance the ride comfort of the vibratory roller under different simulation conditions.

3.4 Experimental study

To verify the study results of the 3D vehicle dynamic model, an off-road vibratory roller with the cab isolation equipped with the HM and seat's PS embedded by the QZSS was used for the experiment. The experiment of the vibratory roller was performed in the condition of the vehicle working on a poor level of the elastoplastic soil ground surface at $v_0 = 1.67$ m/s under the excitation of the drum $f = 28$ Hz. In addition, the calculation parameters of the vibratory roller and elastoplastic soil ground used in the simulation for the experimental study are listed in Tabs. 4 to 6. The experimental model of the vehicle is plotted in Fig. 11. To determine the acceleration and PSD acceleration of the driver's seat, a 3D acceleration sensor of ICP® was installed on the seat to calculate its acceleration response. Then, a dynamic test and analysis system of the Belgium LMS was applied to compute and display the measurement results. The results of the acceleration response and PSD acceleration of the driver's seat are illustrated in Fig. 12.

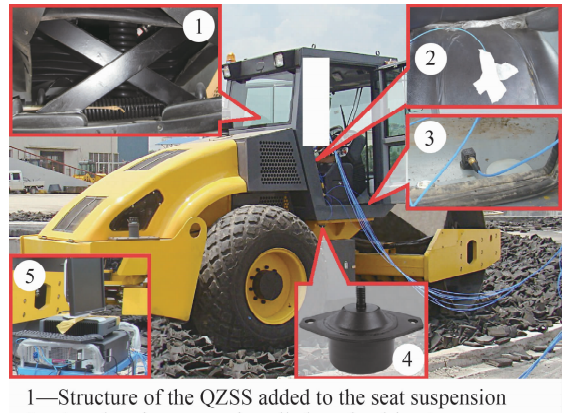

1—Structure of the QZSS added to the seat suspension
2—Acceleration sensor installed on the driver's seat
3—Acceleration sensor installed on the floor of the cab
4—Hydraulic mount of the cab isolations
5—Displacement of the measured results

Fig. 11 Experiment model of the vehicle using the cab's HM and seat's PS added by the QZSS

Fig. 12(a) shows that the seat's acceleration in the numerical simulation is similar to that in the measurement. The calculation result of a_{ws} in the numerical simulation is only higher than the measured result of a_{ws} in the experiment by 8.5%. Moreover, the PSD acceleration response in Fig. 12(b) indicates that the resonance peaks of the PSD acceleration of the driver's seat with the numerical simulation are similar to those of the measurement in all the responses and trends. However, the comparative results between the numerical simulation and measurement in Fig. 12 also show that the acceleration response and PSD acceleration of the driver's seat of the measurement

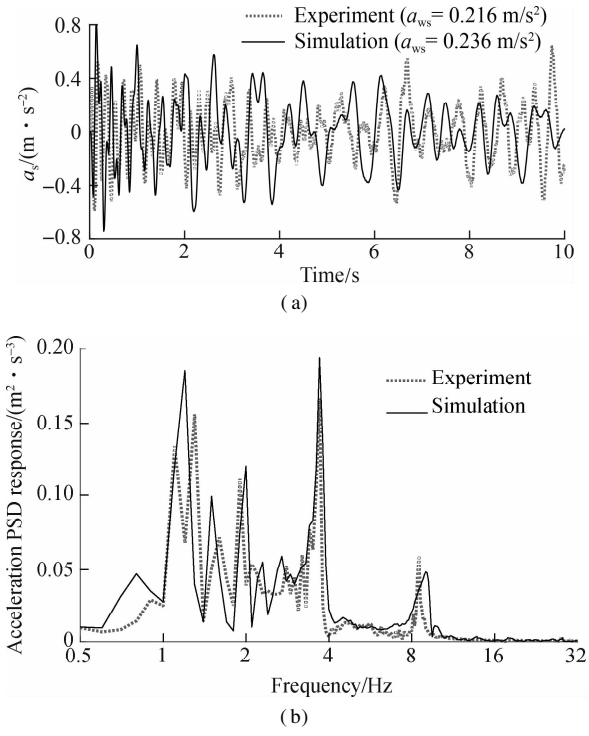

Fig. 12 The measurement result of the seat's vibration response. (a) Seat's acceleration; (b) Seat's PSD acceleration

and numerical simulation have a small error. This result is attributed to the effect of some deviations in the dynamic parameters of the vibratory roller and QZSS. In addition, there was also a small error during the installation of the experimental equipment. However, these errors are very small and insignificantly affect the research results. Therefore, the mathematical model of the vibratory roller and the numerical simulation results are acceptable. Hence, the QZSS embedded in the seat's SAS should be applied to ameliorate the driver's ride quality of off-road vibratory rollers.

4 Conclusions

1) The seat's SAS, controlled by the fuzzy control, significantly improves the vibratory roller's ride comfort compared to the seat's PS, whereas the QZSS added into the seat's PS improves the vehicle's ride comfort better than the seat's SAS.

2) With the QZSS embedded in the seat's SAS, a_{ws} and maximum value of the PSD acceleration of the driver's seat have been markedly decreased compared to the seat's PS, SAS, and PS + QZSS. In particular, the values of a_{ws} and the maximum value of the PSD acceleration of the driver's seat are strongly reduced by 75.7% and 74.3% compared to the seat's PS, respectively.

3) By applying the SAS and QZSS for the driver's seat suspension of the vibratory roller, the results of this study greatly ameliorate the ride comfort of drivers. Therefore, this study not only contributes to the existing body of knowledge on vibratory rollers, but it could also provide an important reference for the application of the QZSS on the semi-active seat suspension of other vehicles to further improve the ride comfort of drivers.

References

[1] Adam D, Kopf F. Theoretical analysis of dynamically loaded soils [C]//*European Workshop Compaction of Soils and Granular Materials*. Paris, France, 2000: 207 − 220.

[2] Le V. *Vibration study and control for cab of vibratory roller* [D]. Nanjing: Southeast University, 2013. (in Chinese)

[3] Nguyen V L, Zhang J R, Yang X Z. Low-frequency performance analysis of semi-active cab's hydraulic mounts of an off-road vibratory roller [J]. *Shock and Vibration*, 2019, **2019**: 1 − 15. DOI: 10.1155/2019/8725382.

[4] Hua W L, Nguyen V L, Zhou H X. Experimental investigation and vibration control of semi-active hydraulic-pneumatic mounts for vibratory roller cab [J]. *SAE International Journal of Vehicle Dynamics, Stability, and NVH*, 2021, **5**(4): 10 − 5. DOI: 10.4271/10-05-04-0028.

[5] International Organization for Standardization. Mechanical vibration and shock-evaluation of human exposure to whole body vibration-Part 2: General Requirement: ISO 2631-1[S]. Geneva, Switzerland: International Organization for Standardization, 1997.

[6] Maciejewski I. Control system design of active seat suspensions[J]. *Journal of Sound and Vibration*, 2012, **331**(6): 1291 − 1309. DOI: 10.1016/j.jsv.2011.11.010.

[7] Bayar K, Khaneghah F S. Optimal sliding mode control method for active suspension control[J]. *IFAC-PapersOnLine*, 2020, **53**(2): 14285 − 14291. DOI: 10.1016/j.ifacol.2020.12.1178.

[8] Li S M, Nguyen V L, Jiao R Q, et al. Isolation efficiency of vehicle seat suspension with three quasi-zero stiffness models [J]. *The International Journal of Acoustics and Vibration*, 2022, **27**(3): 210 − 220. DOI: 10.20855/ijav.2022.27.31858.

[9] Ni D K, Nguyen V L, Li S M. Performance analysis of the seat suspension using different models of the optimal negative-stiffness-structures[J]. *Proceedings of the Institution of Mechanical Engineers, Part D*: *Journal of Automobile Engineering*, 2022: 095440702210910. DOI: 10.1177/09544070221091040.

[10] Palomares E, Nieto A J, Morales A L, et al. Numerical and experimental analysis of a vibration isolator equipped with a negative stiffness system[J]. *Journal of Sound and Vibration*, 2018, **414**: 31 − 42. DOI: 10.1016/j.jsv.2017.11.006.

[11] Zha J L, Nguyen V L, Ni D K, et al. Optimizing the geometrical dimensions of the seat suspension equipped with a negative stiffness structure based on a genetic algorithm [J]. *SAE International Journal of Vehicle Dynamics, Stability, and NVH*, 2022, **6**(2): 147 − 158. DOI: 10.4271/10-06-02-0010.

[12] Zhang X. *Modelling, simulation and optimization of ride comfort for off road articulated dump trucks* [D]. Nanjing: Southeast University, 2013. (in Chinese)

[13] Bekker M G. *Introduction to terrain-vehicle systems*[M]. Ann Arbor, USA: University of Michigan Press, 1969

[14] International Organization for Standardization. ISO/TC108/SC2/WG4 N57 Reporting vehicle road surface ir-

regularities [S]. Stuttgart, Germany: Thieme Medical, Publishers, 1982.
[15] Wong J Y. *Theory of ground vehicles*[M]. 3rd ed. New-York, USA: John Wiley, 2001.
[16] Mitschke M. *Dynamik der Kraftfahrzeuge*[M]. Berlin, Germany: Springer Berlin Heidelberg, 1972. DOI: 10.1007/978-3-662-11585-5.
[17] Mamdani E H, Assilian S. An experiment in linguistic synthesis with a fuzzy logic controller[J]. *International Journal of Human-Computer Studies*, 1999, **51**(2): 135 − 147. DOI: 10.1006/ijhc.1973.0303.
[18] Nguyen V L, Jiao R Q, Zhang J R. Control performance of damping and air spring of heavy truck air suspension system with optimal fuzzy control[J]. *SAE International Journal of Vehicle Dynamics, Stability, and NVH*, 2020, **4**(2): 179 − 194. DOI: 10.4271/10-04-02-0013.

基于 QZSS 和座椅半自动悬架的振动压路机平顺性提升

阮文廉[1,2]　张建润[3]　周华祥[1,2]

([1] 湖北理工学院机电工程学院, 黄石 435003)
([2] 湖北理工学院智能输送技术与装备湖北重点实验室, 黄石 435003)
([3] 东南大学机械工程学院, 南京 211189)

摘要: 为了提高振动压路机的平顺性,提出了一种座椅悬架的半主动悬架(SAS)和准零刚度结构(QZSS)的组合. 建立了 3-D 振动压路机的动力学模型,在弹塑性土壤各种工作条件下,对座椅的 SAS 和 QZSS 进行仿真与性能分析. 将驾驶员座椅的加权加速度均方根值(a_{ws})和功率谱密度加速度(PSD)作为目标函数,进行了试验研究,以验证模型的准确性. 研究结果表明,与座椅的被动悬架相比,座椅的 SAS 显著提高了振动压路机的平顺性,而座椅被动悬架中添加 QZSS 比座椅的 SAS 更能提高平顺性. 特别是 QZSS 添加在座椅 SAS 中,驾驶员座椅的 a_{ws}和最大 PSD 值相比座椅的被动悬架分别降低了 75.7% 和 74.3%. 因此,将 QZSS 添加在座椅 SAS 中,可以进一步提高振动压路机的平顺性.

关键词: 振动压路机;准零刚度结构;半主动悬架;平顺性
中图分类号: U461.3